

# Ultra-Thin Tunable Plasma-Metasurface Composites for Extremely Broadband Electromagnetic Shielding Applications

Ali Abdolali<sup>1, 2</sup>, Maryam Rajabalipanah<sup>3</sup>, and Hamid Rajabalipanah<sup>1, 2, \*</sup>

**Abstract**—For the first time, the concept of combinational use of subwavelength metasurfaces and plasma media is introduced in this paper for being utilized in practical radio frequency (RF) shielding applications. Using an equivalent circuit model, it is demonstrated that the simultaneous use of the lossy characteristic and special dispersion of plasma in low-frequency regime and the transmission zeros provided by spatially homogeneous metasurfaces in the upper frequency band results in superior shielding performances. The designed coating layer has an ultra-thin profile while exhibiting a super wide reject band ranging from 1 to 20 GHz ( $|S_{21}| < -10$  dB). A fair comparison is also performed to elucidate that the proposed plasma-metasurface composite (PMC) shield outperforms the previously reported RF shielding FSSs in both bandwidth and thickness. The numerical results show that while maintaining a low profile, the shielding bandwidth of the designed PMC can be set to surprisingly include all the UHF, L, S, C, X, Ku, and K bands. Moreover, the designed coating layer provides a stable and polarization-insensitive reject band for different incident wave angles up to  $45^\circ$ . These superior performances, as well as the shielding tunability enabled by plasma, confirm the promising capabilities of PMC structures for various applications.

## 1. INTRODUCTION

The ever-increasing advances in electronics and telecommunications industries have improved the human lives in a positive way. Cell phones, electrical apparatus, power lines and wiring systems are examples of instruments whose electromagnetic (EM) radiation endangers human health [1]. Therefore, the need to protect electronic devices and humans against unwanted and harmful electromagnetic waves has been dramatically felt. To meet this need, the electromagnetic interference (EMI) shielding materials have been introduced. The EM coupling between adjacent circuits and controlling the passing or stopping of specific frequencies can be prevented using the shielding devices, providing a safe communication. Recently, many studies have been conducted on high-performance EMI protective materials such as carbon-based materials and metal materials due to their high electrical conductivity [2].

Metasurfaces are the two-dimensional (2D) versions of metamaterials, as a new and more powerful generation of conventional frequency selective surfaces (FSSs), typically organized by arranging subwavelength metal-dielectric inclusions on a flat plane. In recent years, they have been intensely investigated in terms of an abundance of functionalities covering multiple/broadband absorptions [3–6], spatial filtering [7], polarization control [8] antenna engineering [9], wave-manipulation [1–14], radar cross section reduction [15, 16] and cloaking [17]. By setting the electromagnetic (EM) parameters of metasurfaces, one can engineer the amplitude and phase spectra of the reflected and transmitted waves. Nowadays, the concerns about the wideband EMI reduction make researchers survey FSSs as

---

Received 6 April 2018, Accepted 24 June 2018, Scheduled 9 July 2018

\* Corresponding author: Hamid Rajabalipanah (rajabalipanah@elec.iust.ac.ir).

<sup>1</sup> Department of Electrical Engineering Iran University of Science and Technology, Tehran 1684613114, Iran. <sup>2</sup> Applied Electromagnetic Laboratory, School of Electrical Engineering, Iran University of Science and Technology, Tehran 1684613114, Iran.

<sup>3</sup> Department of Electrical Engineering, Amirkabir University of Technology, Tehran 1591634311, Iran.

a spatial signal blocker or attenuator in a certain frequency band ranging from micro- to millimeter-wave [18–26]. Hashemi and Abdolali established FSSs to shield rooms against EM fields in order to achieve secure indoor communications and reduce human exposure to external fields [18]. The secure room was designed using two-layer FSSs with an FR4 substrate to cover 10–12 GHz frequency band, exhibiting 20 dB isolation between inside and outside of the room in the desired frequency band. In [19], a simple and compact FSS configuration was utilized to provide an ultra-wide reject band with more than 20 dB attenuation from 4.6 to 16 GHz. Sivasamy et al. proposed an RF shielding FSS whereby a 20 dB attenuation level at the normal incidence was obtained for a wide bandwidth of 7.53 GHz [20]. The authors of [21] investigated a four-layered FSS configuration, showing a wide reject bandwidth ranging from 2.7 GHz to 13.2 GHz. Mighani and Mallahzadeh designed an FSS platform with the ability of EM shielding whose measurement results showed that the proposed structure had an SE better than 20 dB in 5.1–13.3 GHz frequency range [22]. Using single or multilayer structures, several stop/absorption bands with different operating bandwidths have been achieved [23–30]. Nevertheless, in addition to using complicated geometries, one of the limitations of the restricted shielding bandwidth, angular dependency, not being tunable, thick and heavy profiles circumscribe their practical applications.

Plasma as the fourth state of matter is known as a dispersive and lossy medium [31–33], which introduces wide range electromagnetic (EM) applications. Interaction of EM waves with plasma has already been investigated through different studies. Plasma as an alternative for other EM absorbers exhibits a great reduction of wave power in a large variety of frequencies and incident angles. Owing to the reconfigurable operation, i.e., ON or OFF, plasma has been found as an especial placement between other natural materials, especially in wave manipulation engineering [34, 35]. More recently, according to the interesting features enabled by the plasma mediums, different combinations with the other artificial structures have been reported for them, leading to substantial improvements in the overall performances [36–39]. For instance, Yuan et al. designed a multilayer radar-absorbing structure with plasma- and radar-absorbing material (RAM) to investigate the stealth mechanisms of a multilayer absorber [36]. By a combination of plasma and resistive frequency-selective surface (FSS), a wideband absorber was reported in [37], spanning both the X- and Ku-bands. Plasma and metallic FSSs have been analytically studied to achieve a proper reflection phase interval, improving the checkerboard surface to reduce the bistatic radar cross section (RCS) of a metal plate [38]. In one of our previous researches, we conducted a theoretical study to introduce a new type of low-thickness and ultra-broadband stealth platforms by the combinational use of plasma medium and graphene sheets for the first time [39]. Following the above-mentioned references, here, we seek to reveal a proper hybrid use of plasma and metasurfaces to be elaborately established in the current EM shielding applications. To the best of our knowledge, such a specified application by combining the metasurfaces and plasmas has not been reported yet.

In the present study, based on the combinational use of spatially homogeneous metasurfaces and thin plasma substrates, a new type of ultra-thin RF shielding panels is studied, providing extremely broad reject band. The absorptive property of the plasma and transmission zeros provided by the designed metasurfaces in the lower and upper frequency bands respectively are simultaneously exploited as the main idea of this paper. The proposed plasma-metasurface composite (PMC) shield is simple, in low profile, and feasible while consisting of three subwavelength square loop metasurfaces embedded between two plasma substrates. A comprehensive parametric study along with an equivalent circuit model is accomplished to demonstrate the effects of each layer on the total shielding performances. The tunable property of plasma allows a reconfigurable shielding response over the frequency band of study. The numerical results illustrate a super wide reject band ranging from 1 to 20 GHz (181%) ( $|S_{21}| < -10$  dB), spanning all the UHF, L, S, C, X, Ku, and K frequency bands. The results of PMC RF shield obviously overcome those previously reported in similar references from the aspects of both the operating bandwidth and thickness.

## 2. ELECTROMAGNETIC MODELLING OF PMC

As an amazing property, plasma has dispersive lossy constitutive parameters, enabling a great opportunity for being utilized in diverse EM applications. In the format of the well-known Drude model, the complex relative permittivity of the cold collision weakly ionized plasma can be expressed

as [40]:

$$\epsilon_r = 1 - \frac{\omega_p^2}{\omega(\omega - i\nu_p)} \quad (1)$$

Here  $\omega = 2\pi f$  is the incident wave frequency, and  $\omega_p$  and  $\nu_p$  are the plasma and collision frequencies, respectively, which can be expressed as:

$$\omega_p = \sqrt{\frac{n_0 e^2}{m_e \epsilon_0}} \quad (2)$$

$$\nu_p = \frac{4}{3} \pi \alpha^2 N \nu_{av} \quad (3)$$

where  $n_e$  is the equilibrium electron density,  $e$  the electron charge ( $= 1.6 \times 10^{-19}$ ), and  $m_e$  the electron mass ( $= 0.91 \times 10^{-30}$ ). Eq. (3) is obtained according to the statistical theory [41] in which  $N$  is the number density, and  $\nu_{avg}$  is the average velocity of electron. Conventional metasurfaces are composed of periodic metallic patterns printed on a specified dielectric spacer. These artificially constructed structures are usually illuminated by a plane wave and exhibit a certain response in different frequency bands. Since the plasma layers are utilized as the supporting substrates in this paper, their EM properties should be taken into account under a plane wave excitation. The schematic view of assumed configuration is depicted in Figure 1. A plane wave in plasma, similar to other lossy mediums, obeys Maxwell equations, where with assuming  $\exp(j\omega t)$  in the time domain, the propagating wave can be obtained as:

$$E(z, t) = E_0 \exp(j\omega t - \gamma z) \quad (4)$$

where  $\gamma = 2\pi f \sqrt{\epsilon_r}/c$  is the complex propagation constant. We assume that the  $z$ -direction is perpendicular to the PMC. Similar to most of the preceding researches [18–26], the normal incidence case is only studied for the initial design steps. However, the angular stability of the final PMC RF shield will be evaluated under different incident wave angles in both TE and TM polarizations. The proposed PMC shield is composed of three square-loop metasurfaces embedded between two thin plasma layers with the thicknesses of  $t_1$  and  $t_2$ . The total thickness of RF shielding panel is  $t = t_1 + t_2$ . Unlike full-wave simulations, a circuitual analysis reveals immediate results and important physical insights into the design properties of the PMC RF shield. The supporting plasma layers can be modelled as dispersive lossy transmission lines with the characteristic impedance of  $Z_{ci} = Z/\sqrt{\epsilon_{ri}}$  ( $Z \approx 120\pi$ ) [39]. The transmission line model of the proposed PMC composite is depicted in Figure 2 where the lossless square-loop metasurfaces are represented by parallel admittances ( $jB_{s,i}$ ). As a result, by multiplying

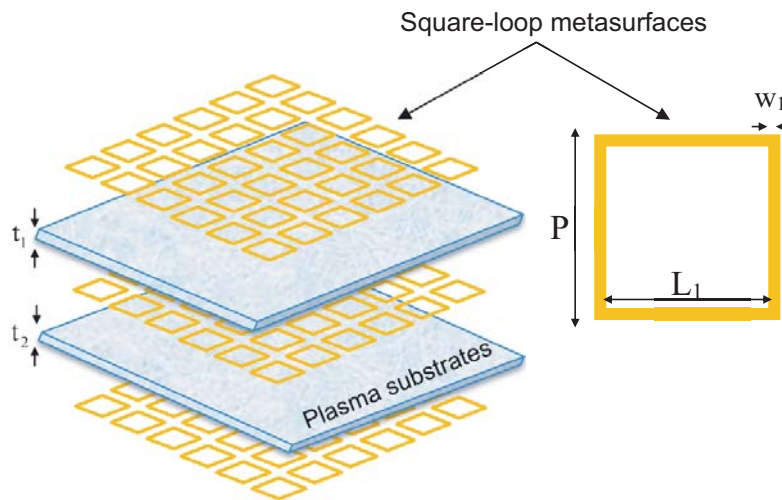


**Figure 1.** The employed multilayer PMC RF shield with the total thickness of  $t = t_1 + t_2$ .

all the transmission matrices ( $ABCD$ ), we have:

$$T_{tot} = \begin{bmatrix} A & B \\ C & D \end{bmatrix} = T_{meta,1} \times T_{sub,1} \times T_{meta,2} \times T_{sub,2} \times T_{meta,3} \quad (5)$$

hereupon:

$$T_{meta,i} = \begin{bmatrix} 1 & 0 \\ jB_{S,i} & 1 \end{bmatrix} \quad (6)$$

$$T_{Sub,i} = \begin{bmatrix} \cosh(\gamma_i t_i) & Z_{C,i} \sinh(\gamma_i t_i) \\ \sinh(\gamma_i t_i)/Z_{C,i} & \cosh(\gamma_i t_i) \end{bmatrix} \quad (7)$$

where,  $B_{S,i} = \omega C_i - 1/\omega L_i$  Consequently, the reflection ( $R$ ) and transmission ( $T$ ) coefficients of total structure can be extracted by:

$$R = S_{11} = \frac{A + B/Z_0 - CZ_0 - D}{A + B/Z_0 + CZ_0 + D} \quad (8)$$

$$T = S_{21} = \frac{2}{A + B/Z_0 + CZ_0 + D} \quad (9)$$

As Figure 2 implies, the PMC structure has input and output ports, thereby falling into the category of two-port networks. In this paper, we mainly focus on the RF shielding problem, and the magnitudes, i.e.,  $|R|$  and  $|T|$ , are only considered. To clarify the validity of the proposed equivalent circuit model, a PMC structure with arbitrary parameters given in the caption of Figure 3 is considered and simulated. The commercial software, CST Microwave Studio 2017, is utilized as the full-wave EM solver where the unit cell boundaries are applied to the  $x$  and  $y$  directions, and the Floquet ports are also assigned to the  $z$  direction.

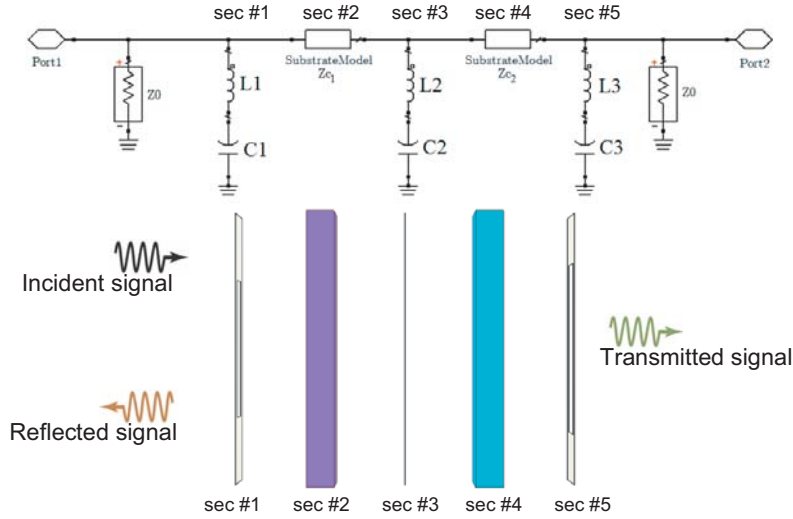


**Figure 2.** The equivalent circuit model of the proposed multilayer PMC RF shield with the total thickness of  $t_1 + t_2$ . The setup of simulations is schematically drawn in the bottom figure.

A plane wave incidence normally impinges on the PMC shield from one side, and the spectral domain of the reflected and transmitted signals are recorded (see Figure 2). Besides, the components of equivalent circuit model are determined so that an acceptable agreement is observed between the results of the equivalent circuit model and those of the full-wave simulations. The results are compared in Figure 3. According to this figure, one can conclude that the equivalent circuit model of Figure 2 can successfully follow the trend of the full-wave simulation results. Indeed, the physical basis of the PMC performance and the provided resonances are well recognized and predicted by the proposed equivalent circuit model. The null resonances originate from the metasurfaces, and the insertion loss observed

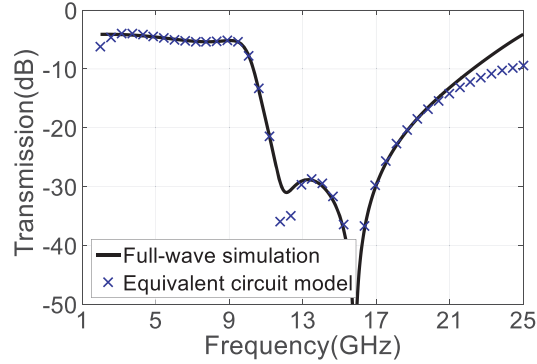


**Figure 3.** The transmission spectra of the PMC structure obtained with different methods (equivalent circuit model and full-wave numerical simulation).

in the low frequency region arises from the plasma lossy substrates. A comprehensive discussion will be given in the following section. The slight discrepancy in the upper frequency region can also be attributed to three main issues. 1) high frequency inductive and capacitive mutual couplings between the metasurface layers; 2) neglecting the dispersive behavior of the lumped circuit elements, which is very crucial at higher frequency band, and 3) ignoring the high order Floquet harmonics, which is very important at the same frequency band. Indeed, the agreement between the circuit model and full-wave results is satisfactory if the periodicity of spatially homogeneous metasurface is smaller than the operating wavelength [42].

### 3. ULTRA-BROADBAND PMC RF SHIELD AND ITS PRINCIPAL MECHANISM

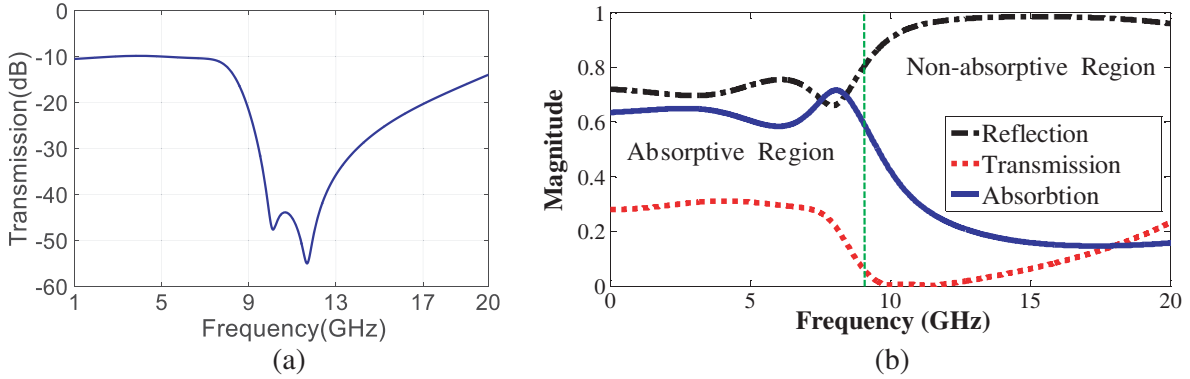
As already mentioned, the proposed PMC shield consists of three square-loop metasurfaces supported by two plasma spacers. Armed with a series LC circuit model, the square loop metasurfaces provide several transmission zeros at different locations of spectral domain, which will be exploited in the present study in order to achieve a wide band-stop shielding response. Evidently, by appropriate choosing of plasma parameters and geometric specifications of square loop metasurfaces as the constitutive elements of the designed PMC, one can arbitrarily engineer the reflection and transmission coefficients of Eq. (9). It is assumed that the plasma layers and metasurface admittances are independently adjusted to yield the desired transmission spectrum. According to the ratio of plasma and collision frequencies, the real part of permittivity would be less than one and could even be negative [39]. This unique property along with being lossy can lead to an extensive range of wideband EM applications when it is combined with the versatile metasurfaces. Regarding the  $\text{Re}(\epsilon_r) < 1$ , the plasma substrates enhance the shielding bandwidth and can also contribute to putting further space between the multiple transmission zeros to span a larger area of the spectral domain. The reason for this is that the input impedance of structure has a smoother response when the plasma substrates are utilized. The previous experimental demonstrations [43, 44] allow the plasma parameters employed in the present study to be freely chosen in the validity ranges of  $1 \times 10^{10} < \omega_p < 6 \times 10^{10}$  and  $1 \times 10^6 < \nu_p < 1 \times 10^{11}$ . By properly adjusting the parameters, the metasurfaces are designed to exhibit a broadband impedance mismatch in the upper frequency range, and the plasma medium parameters are adjusted so that a wideband attenuation in the lower frequency region is guaranteed. The impedance mismatch would lead to multiple transmission zeros governed by the square loop metasurfaces. It should be noted that providing transmission zeros at low frequencies by solely establishing the metasurfaces requires bulky and thick profiles [21], which is not desired in the real-life scenarios. This is the reason that the plasma lossy features are alternatively utilized to attenuate the low frequency incident signals. The optimum parameters of the designed PMC RF shield are given in Table 1.

The optimized PMC shield is simulated using CST Microwave Studio 2017, and the overall transmission spectrum is extracted in Figure 4(a). As can be observed, the EM signals impinging on the PMC RF shielding panel experience at least 10 dB attenuation in an ultra-broad frequency band

**Table 1.** The optimum parameters of the proposed PMC RF shield.

$P$	$L_1$	$L_2$	$L_3$	$w_1$	$w_2$	$w_3$
10 mm	6.2 mm	7.8 mm	5 mm	1.8 mm	1 mm	2.4 mm
$t_1$	$t_2$	$\omega_{p1}$	$\omega_{p2}$	$\nu_{p1}$	$\nu_{p2}$	
1 mm	1 mm	$4.1 \times 10^{10}$ rad/s	$4.1 \times 10^{10}$ rad/s	$4.9 \times 10^{10}$ Hz	$3.9 \times 10^{10}$ Hz	

from 1 to 20 GHz when passing through the structure, and this value becomes more than 20 dB between 9 and 17 GHz. To better understand the principal mechanism, the transmission, reflection and absorption spectra of the proposed PMC are also computed by  $A = 1 - |S_{11}|^2 - |S_{21}|^2$  [5] and shown in Figure 4(b) to elucidate the physics behind such superior performance. Owing to the high imaginary part of the permittivity appearing in the frequency range of 1–9 GHz, the PMC RF shield dissipates the trapped wave in the same frequency band, making a remarkable attenuation in the incident radiations. On the other hand, multiple transmission zeros arising from square loop metasurfaces also provide the desired impedance mismatch so that a wide band-stop response in the range of 9–20 GHz is acquired whereby most portion of the power-signal is reflected back. Hence, when a radiative signal covering a broad frequency spectrum impinges on the PMC RF shield, it is just as the illuminated wave going through a resistive-inductive-capacitive (RLC) spatial filtering panel. Regarding the filtering and lossy behavior, different resonances are excited resulting in passing, dissipating or blocking special frequency ranges. By a combination of these physical phenomena as the main idea of this paper, an extremely broadband shielding response against the incident signals is obtained via the proposed design. Nevertheless, the effects of these transmission zeros and the lossy characteristics of the plasma can be observed in a negligible form in the other frequency regions.

**Figure 4.** (a) The transmission spectra of the optimum PMC shield. (b) Three different operational regions in the performance of the proposed PMC RF shield.

As revealed earlier, having a compact size and exhibiting a broader stop-band are two crucial factors affecting the overall performance of a specific RF shield. To clarify the superior performances of the designed PMC structure, it is compared with some of the recent designs archived in the literature. They are fairly compared for the factors of thickness, bandwidth, and tunability. As depicted in Table 2, [21, 26, 27, 30], 37] contribute to a heavy and thick profile with respect to the presented work. Despite occupying a larger space, these configurations result in a smaller attenuation bandwidth rather than the design proposed in the present study. The designed configurations in [16, 18, 22, 24, 25, 28, 29] have a reasonable thickness; however, their rejected bandwidths are significantly lower than the operating band of the PMC shield in this work. In addition to maintaining a reasonably thick profile, [19, 20, 23] offer a broad attenuation band. Nevertheless, in addition to lower operating bandwidth than this paper, no tunable shielding responses have been reported for them. This is where the proposed PMC design demonstrates a superior performance and wider bandwidth through a low-thickness and tunable

**Table 2.** A fair comparison between the shielding performances reported in this paper and the reject/absorption bandwidths presented in the recently published references.

Reference	Shielding Band (GHz) ( $ S_{21}  < -10$ dB)	Fractional Bandwidth (%)	Polarization	Total Thickness	Tunability
Ref. [16]	8.2–23.1	95%	Both of TE&TM	3 mm	×
Ref. [18]	9–14	43%	Both of TE&TM	3 mm	×
Ref. [19]	4.6–16	110%	Both of TE&TM	1.6 mm	×
Ref. [20]	4–14	111%	Both of TE&TM	1.6 mm	×
Ref. [21]	2.7–13.2	132%	Both of TE&TM	11 mm	×
Ref. [22]	5.3–16.1	89%	Both of TE&TM	3.2 mm	×
Ref. [23]	3.1–10.6	106%	Both of TE&TM	2.4 mm	×
Ref. [24]	8–18	80%	Both of TE&TM	0.6 mm	×
Ref. [25]	40–70	54%	Both of TE&TM	0.5 mm	×
Ref. [26]	5–16	104%	Both of TE&TM	4.2 mm	×
Ref. [27]	4.4–18	121.4%	Both of TE&TM	10 mm	×
Ref. [28]	2.5–5	67%	Both of TE&TM	2 mm	×
Ref. [29]	8–18	77%	Both of TE&TM	2.5 mm	×
Ref. [30]	4–16.9	123%	Both of TE&TM	10 mm	×
Ref. [37]	8–18	77%	Both of TE&TM	27.4 mm	✓
<b>This work</b>	1–20	181%	Both of TE&TM	2 mm	✓

configuration. In addition, a deep attention to the investigated literature illustrates good operating and promising features making the PMC RF shield a suitable option in real-world implementations. The tunable performance of the proposed PMC RF shield will be investigated in the following section.

#### 4. PARAMETRIC STUDY

Different parameters have been considered in designing the PMC RF shield (see Figure 1). The geometry of metasurfaces and substrate parameters are some of the key factors forming the final transmission curve for a typical RF shield. Evidently, to confirm the flexibility of design, we discuss the effects of each geometric parameter on the transmission spectrum of the proposed PMC RF shield. During our simulations, only one parameter is varied around its reference while the others remain constant. The reference parameters of the PMC structure are the optimized ones listed in Table 1. Firstly, the total thickness ( $t = t_1 + t_2$ ) of the structure is changed around ( $t = 2t_1 = 2t_2 = 2$  mm), and the effect of its variation on the  $S_{21}$  curves is investigated and plotted in Figure 5(a). The numerical simulation is accomplished when the thickness is changed in the range of  $1 \text{ mm} < t < 4 \text{ mm}$  with a step width of 1 mm. As expected by increasing the plasma thickness, the incident EM signal experiences a greater attenuation when propagating in the plasma dielectrics. Such an issue is not dedicated to a specified frequency region and affects the whole spectrum (see Figure 5(a)). Increasing the total thickness of PMC is a possible solution if more attenuation levels are demanded, especially in the low frequency region. Secondly, the transmission spectra of the PMC shield are evaluated for different lengths of the square loop metasurface located in the top, middle and bottom layers, and the corresponding results are shown in Figures 5(b)–(d) respectively. As already mentioned, the length of square loops plays an important role in constructing their inductive behaviour. Varying each length can contribute to change in one of the resonance frequencies while the other remains almost unchanged. The increase in the length of metasurfaces leads to a proportional increase in the inductances and capacitances of the branches in the circuit model, thereby reducing the corresponding resonance frequencies. By putting these frequencies close to or far from each other, which can be noticed by changing the length of loops, one can imagine different isolation levels ( $>$  or  $<$  20 dB) between the transmitting and receiving ports, especially in the center frequency region. For instance, from Figure 5(b), one can conclude

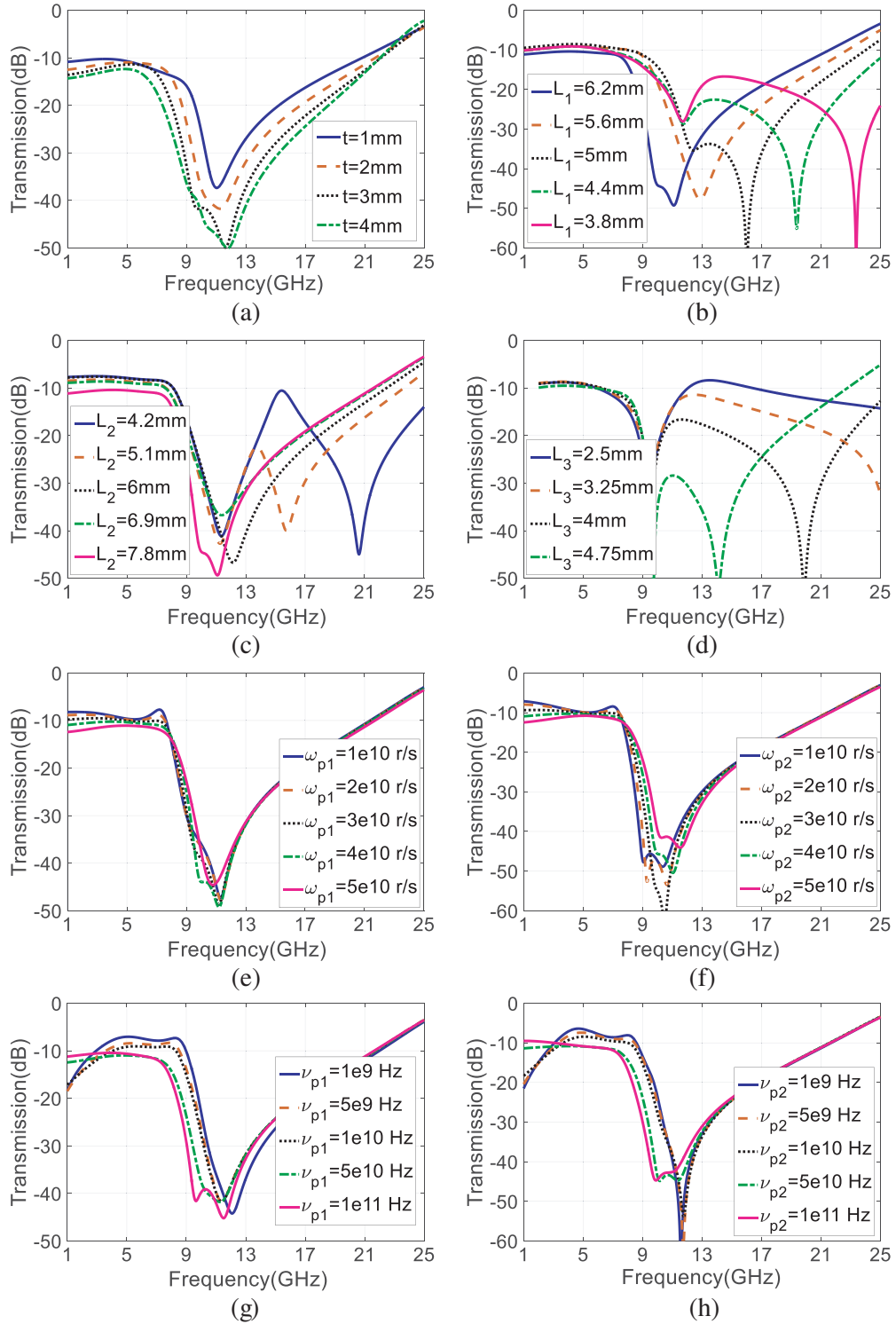


**Figure 5.** The transmission spectra of the designed PMC RF shield at normal incidence and for different: (a) thicknesses, (b) lengths of the square loop metasurface at the top layer; (c) lengths of the square loop metasurface at the middle layer; (d) lengths of the square loop metasurface at the bottom layer; (e) plasma frequencies of the top plasma layer; (f) plasma frequencies of the bottom plasma layer; (g) average collision frequencies of the top plasma layer; (h) average collision frequencies of the bottom plasma layer.

that by setting  $L_1 = 3.8$  mm, the second resonance shifts toward higher frequencies, yielding a super-wide reject band ( $|S_{21}| < -10$  dB) from 1 GHz to more than 25 GHz but at the expense of a weaker isolation between the Floquet ports. Because of the great influence on the wave propagation, the impact of plasma and collision frequencies for each layer should also be elucidated. As an interesting property, the plasma and collisional frequency can be electrically tuned by the variation of electron density [39]. Regarding the practical ranges of plasma parameters, the plasma and collision frequencies are changed in the ranges of  $1 \times 10^{10}$  rad/s  $< \omega_p < 5 \times 10^{10}$  rad/sec and  $1 \times 10^9$  Hz  $< \nu_p < 1 \times 10^{11}$  Hz, respectively. We continue the study by changing these parameters and assessing their effects on the shielding performance of the designed PMC structure. As shown in the insets of Figures 5(e) and (f), the parameters of  $\omega_{p1} = \omega_{p2} = 5 \times 10^{10}$  rad/sec enable the best shielding attenuations at the lower part of the spectrum. At this frequency range, a larger electron density results in a stronger absorption, and finally, at the higher frequencies, the absorption behavior of the plasma medium has been eliminated [39]. Although varying the plasma parameters slightly affects the other frequency regions, it can be accounted as a suitable degree of freedom in controlling the attenuation level of the low-frequency band (almost  $< f = 9$  GHz). On the other hand, up to a certain frequency, the absorption behavior of the structure is significantly affected by the variation of average collision frequency. A larger average collision frequency has a higher absorption rate [39]. However, by increasing the frequency, the effects of average collision frequency variation disappear (see Figures 5(g), (h)). Therefore, one can envision a tunable shielding response for the proposed PMC RF shield by means of an external electrical biasing circuit.

Eventually, from numerical simulations, it is demonstrated that different parameters can affect the shielding performance of the designed PMC. Indeed, by properly adjusting them, the shielding bandwidth can be further broadened to surprisingly include all the UHF, L, S, C, X, Ku, and K bands. Apart from suitable scattering parameters, providing stable response against different angles of incidence for both TE and TM polarizations (AOI) is a key requisite in the design of RF shield. This section drills down the effect of different AOIs on the proposed PMC shielding behavior. Figures 6(a) and (b) show the attenuation level of the incident signal at different AIOs for both TE and TM polarizations. The horizontal axis denotes frequency while the vertical axis refers to transmission coefficient ( $|S_{21}|$ ). The geometrical and EM parameters of the structure are listed in Table 1. As depicted, the proposed PMC RF shield provides a stable and polarization-insensitive reject band for different AIOs up to  $45^\circ$ . The slight deterioration of the results at high frequencies can be attributed to the regions in which the grating lobes occur because of propagation of higher order Floquet modes [42]. In summary, results obviously show that the scattering behavior of the structure does not significantly change with the variation of angles and polarizations, which is of great importance in real-world applications, where different incident angles and polarizations may be encountered.

The physical effect of each metasurface in generating the existing resonances is further explored through scrutinizing the electric and magnetic field distributions at 10.2 GHz and 11.7 GHz (the first and second resonances, respectively), as illustrated in Figures 7(a)–(d). For the sake of brevity, the TE-polarized normal incidence is only considered here. As depicted in the insets of Figures 7(a)

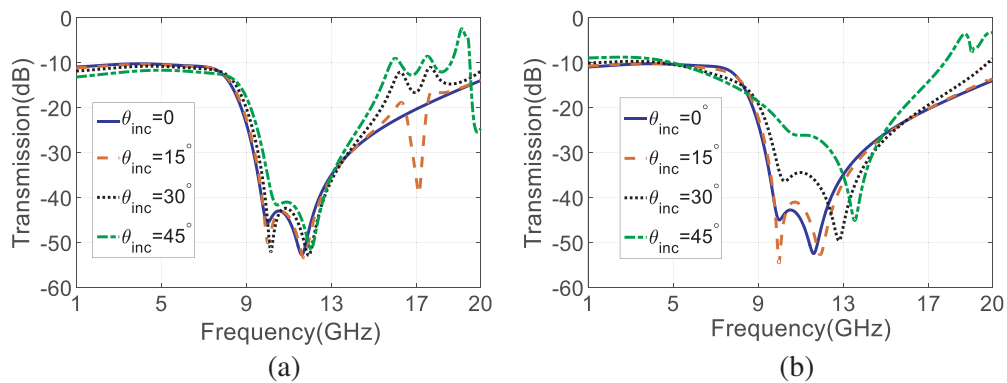


**Figure 6.** The transmission spectra of the proposed PMC RF shield under different angles of (a) TE- and (b) TM-polarized oblique incidences.

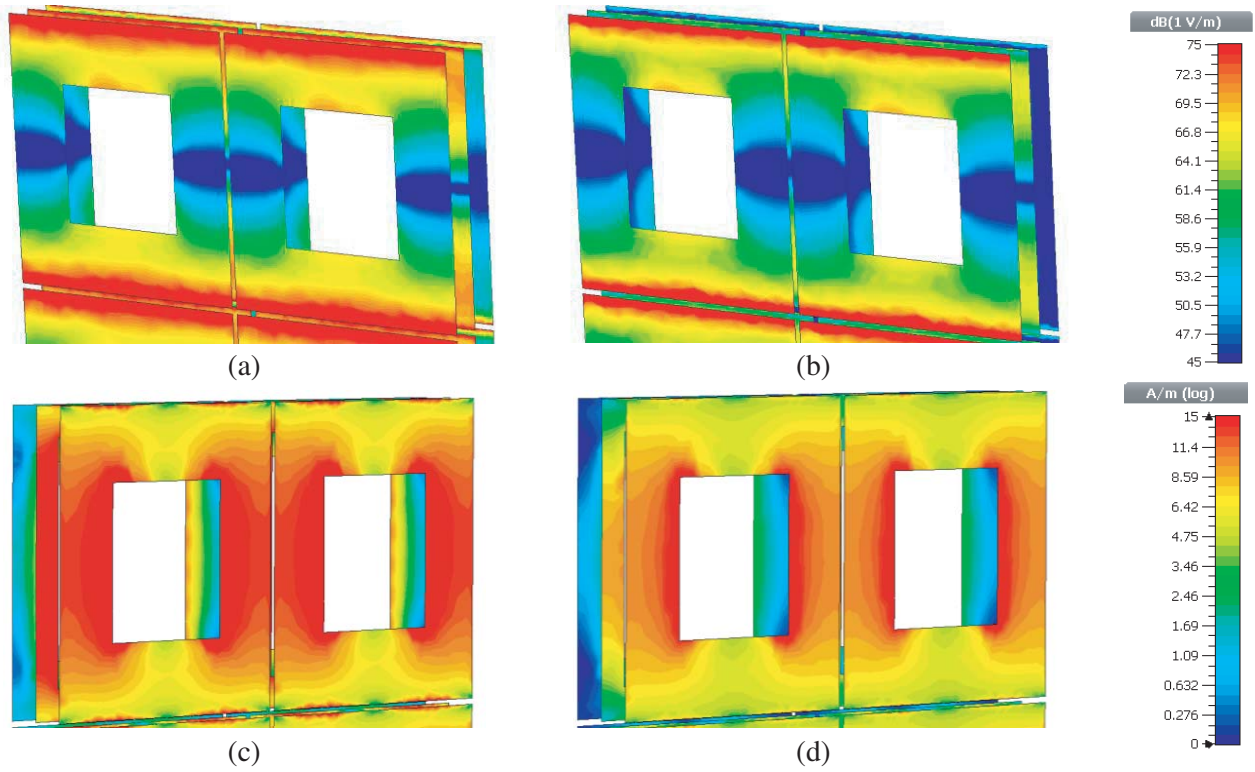


**Figure 7.** The induced electric and magnetic fields on square-loop metasurfaces: (a) the electric field distribution at  $f = 10.2$  GHz; (b) the electric field distribution at  $f = 11.7$  GHz; (c) the magnetic field distribution at  $f = 10.2$  GHz; (d) the magnetic field distribution at  $f = 11.7$  GHz;.

and (b), the induced electric fields are mainly accumulated around the upper and lower edges of the square-loop metasurfaces, thereby constructing the cell capacitance of the circuit model of Figure 2. While Figures 7(a) and (b) demonstrate the contribution of all three metasurfaces in eliminating the transmission, it can be noticed that the third layer has less contribution at  $f = 11.7$  GHz. Besides, the impact of the third resonator greatly increases at  $f = 10.2$  GHz, and the first layer is more effective in eliminating the passing wave in the both resonance frequencies. Figures 7(c) and (d) reveal the magnetic field distributions of the cells where the main resonances around  $f = 10.2$  GHz and  $f = 11.7$  GHz originate from the surface current flow on the vertical arms of the square-loop metasurfaces, yielding the equivalent inductances in the circuit model of Figure 2. Theoretically speaking, the resonance located around  $f = 11.7$  GHz appears due to the existence of the front square-loop metasurface whereas  $f = 10.2$  GHz resonance is excited by the middle layer. The enhanced reflection covering the stopband resonance arises from the impedance mismatch assisted by the third metasurface layer. Moreover, in the higher or lower frequency range, i.e., in out of the stopband provided by the metasurfaces, the magnetic field distribution (or induced surface currents) becomes remarkably weak. Eventually, by exploiting both capacitive and inductive behaviors the proposed PCM RF shield eliminates the transmission in an ultra-broad frequency range from 1 to 20 GHz.

Finally, it should be noted that a feasible fabrication process is imagined for the proposed PCM shield as described below. The plasma FSS consists of a background metal, a plasma dielectric, and a glass cover. A cold collisional weakly ionized plasma is supposed to be confined with glass. The plasma parameters would be sustained with a dc discharge Argon plasma and high-voltage power. The ionizing source can be chosen according to gas type, pressure, and geometry. According to the ideal gas law, the former case leads to the plasma pressure of 163.9 torr while the latter results in the pressure of 86.5 torr regarding the room temperature. In many experimental studies, the plasma gas is confined in a special container. Ref. [32] reported the average collision frequency to the gas number density ratio of different

gas types. For instance, to produce an average collision frequency of 40 GHz at the room temperature, the container should be filled with helium (He) gas that its number density should be  $5.26 \times 10^{18} \text{ cm}^{-3}$ . As another example, to achieve an average collision frequency of 50 GHz at  $T = 300 \text{ K}$ , the number density of Kr should be set as  $2.77 \times 10^{18} \text{ cm}^{-3}$ . Various laboratory strategies such as electron-beam impact ionization and photoionization of a seed gas have been proposed to synthesize a uniform or non-uniform cold plasma [33, 45]. Photoionization is a physical process caused by the interaction between a photon and an atom or molecule and can be performed by a laser source or Spark Board. Numerous applications requiring efficient photoionization of large volumes have utilized Spark Board arrays. The plasma can be synthesized by the photoionization of tetrakis (dimethylamino) ethylene (TMAE) vapor seeded in a purified helium gas [45, 46]. It was demonstrated that the electron density distribution is more uniform along the surface by expanding the Spark Board under the plasma container [33]. The required power per unit volume to sustain a noble gas plasma can be approximately determined by  $P/V = KN_e^2 E_i$  [32]. Here,  $N_e$  is the electron density of the plasma,  $V$  the volume of the plasma,  $P$  the power deposited in the plasma,  $k$  the rate constant for dissociation of the organic vapor, and  $E_i$  the energy to generate an electron-ion pair. In addition, the energy of photoionization and the rate constant for TMAE are estimated as  $E_i = 7 \text{ eV}$  and  $K = (9 \pm 1.1) \times 10^{-6} \text{ cm}^3/\text{s}$ , respectively [32, 45]. In our design, with assuming the plasma frequencies of  $4.1 \times 10^{10} \text{ rad/sec}$  for both upper and bottom layers which yield an electron density of  $N_e = 5.27 \times 10^{18} \text{ cm}^3$  and a highly efficient Spark Board, the necessary power per volume is simply computed as  $2800 \text{ kW/m}^3$ . Besides, the metasurface of the proposed PCM RF shielding structure can be served as metal films of spark board, whose surrounding cells are connected to charged capacitors by proper switching. Consequently, sparks are produced between the array of gaps of metasurface, generating an intense UV light source. An ultra-thin layer of Glass (Pyrex) ( $\epsilon_r = 4.82$  and  $\tan \delta = 0.0054$ ) layer can be imagined as the glass dielectric cover of plasma-filled medium. In our design, the PCM shield is assumed to be infinitely extended toward both horizontal and vertical directions; nevertheless, it is practically composed of a finite-size array of unit elements. Thus, the total dissipated power directly depends on the number of occupying cells [37]. Moreover, an array of UV lasers of a certain size aperture can be established at one side of the structure, instead of using sparkboard to produce the plasma gas.

## 5. CONCLUSION

This research proposes the concept of combinational use of metasurfaces and plasma media as an efficient design of RF shields, which is validated through the numerical and equivalent circuit analyses. The proposed PMC configuration is revealed to be simple, compact and ultra-thin ( $10 \text{ mm} \times 10 \text{ mm} \times 2 \text{ mm}$ ). It is shown that in addition to maintaining a low profile, the operating bandwidth of the designed PMC can be set to surprisingly include all the UHF, L, S, C, X, Ku, and K bands. A fair comparison is also done to elucidate that the proposed PMC platform outperforms the previously reported RF shields from both the bandwidth and thickness aspects. It is proved that the aforementioned PMC structure with small dimensions and single layer exhibits more than 20 dB attenuation in the considered frequency band. Eventually, the suitable performance of the designed PMC shield in real-world applications is confirmed as it provides a stable and polarization-insensitive reject band for different AIOs up to  $45^\circ$ . Therefore, the presented structure is an ideal choice for utilizing in the future ultra-wideband EM shielding applications.

## REFERENCES

1. Agarwal, A., et al., "Effect of cell phone usage on semen analysis in men attending infertility clinic: An observational study," *Fertility and Sterility*, Vol. 89, No. 1, 124–128, 2008.
2. Im, J. S., et al., "Effective electromagnetic interference shielding by electrospun carbon fibers involving  $\text{Fe}_2\text{O}_3/\text{BaTiO}_3/\text{MWCNT}$  additives," *Materials Chemistry and Physics*, Vol. 124, No. 1, 434–438, 2010.
3. Rahmzadeh, M., H. Rajabalipanah, and A. Abdolali, "Multilayer graphene-based metasurfaces: Robust design method for extremely broadband, wide-angle, and polarization-insensitive terahertz absorbers," *Applied Optics*, Vol. 57, No. 4, 959–968, 2018.

4. Cheng, Y. Z., et al., "Ultra-thin multi-band polarization-insensitive microwave metamaterial absorber based on multiple-order responses using a single resonator structure," *Materials*, Vol. 10, No. 11, 1241, 2017.
5. Vahidi, A., H. Rajabalipanah, A. Abdolali, and A. Cheldavi, "A honeycomb-like three-dimensional metamaterial absorber via super-wideband and wide-angle performances at millimeter wave and low THz frequencies," *Applied Physics A*, Vol. 124, No. 4, 337, 2018.
6. Mehrabi, M., H. Rajabalipanah, A. Abdolali, and M. Tayarani, "Polarization-insensitive, ultra-broadband, and compact metamaterial-inspired optical absorber via wide-angle and highly efficient performances," *Appl. Opt.*, Vol. 57, 3693–3703, 2018.
7. Abbaspour-Tamijani, A., K. Sarabandi, and G. M. Rebeiz, "Antenna-filter-antenna arrays as a class of bandpass frequency-selective surfaces," *IEEE Transactions on Microwave Theory and Techniques*, Vol. 52, No. 8, 1781–1789, 2004.
8. Zhu, X.-C., et al., "Design of a bandwidth-enhanced polarization rotating frequency selective surface," *IEEE Transactions on Antennas and Propagation*, Vol. 62, No. 2, 940–944, 2014.
9. Lee, Y. J., et al., "Design of a high-directivity Electromagnetic Band Gap (EBG) resonator antenna using a Frequency-Selective Surface (FSS) superstrate," *Microwave and Optical Technology Letters*, Vol. 43, No. 6, 462–467, 2004.
10. Rouhi, K., H. Rajabalipanah, and A. Abdolali, "Real-time and broadband terahertz wave scattering manipulation via polarization-insensitive conformal graphene-based coding metasurfaces," *Annalen der Physik*, Vol. 530, No. 4, 1700310, 2018.
11. Zhang, K., et al., "Experimental validation of ultra-thin metalenses for N-beam emissions based on transformation optics," *Applied Physics Letters*, Vol. 108, No. 5, 053508, 2016.
12. Momeni, A., K. Rouhi, H. Rajabalipanah, and A. Abdolali, "An information theory-inspired strategy for design of re-programmable encrypted graphene-based coding metasurfaces at terahertz frequencies," *Scientific Reports*, Vol. 8, No. 1, 6200, 2018.
13. Zhang, K., Y. Yuan, D. Zhang, X. Ding, B. Ratni, S. N. Burokur, M. Lu, K. Tang, and Q. Wu, "Phase-engineered metalenses to generate converging and non-diffractive vortex beam carrying orbital angular momentum in microwave region," *Opt. Express*, Vol. 26, 1351–1360, 2018.
14. Zhang, K., et al., "Anomalous three-dimensional refraction in the microwave region by ultra-thin high efficiency metalens with phase discontinuities in orthogonal directions," *New Journal of Physics*, Vol. 16, No. 10, 103020, 2014.
15. Cheng, Y., et al., "An ultra-thin dual-band phase-gradient metasurface using hybrid resonant structures for backward RCS reduction," *Applied Physics B*, Vol. 123, No. 5, 143, 2017.
16. Rajabalipanah, H., H. Hemmati, A. Abdolali, and M. Amirhosseini, "Circular configuration of perforated dielectrics for ultra-broadband, wide-angle, and polarization-insensitive monostatic/bistatic RCS reduction," *IET Microwaves, Antennas & Propagation*, 2018.
17. Alù, A., "Mantle cloak: Invisibility induced by a surface," *Physical Review B*, Vol. 80, No. 24, 245115, 2009.
18. Hashemi, S. and A. Abdolali, "Room shielding with frequency-selective surfaces for electromagnetic health application," *International Journal of Microwave and Wireless Technologies*, Vol. 9, No. 2, 291–298, 2017.
19. Majidzadeh, M., C. Ghobadi, and J. Nourinia, "Ultra wide band electromagnetic shielding through a simple single layer frequency selective surface," *Wireless Personal Communications*, Vol. 95, No. 3, 2769–2783, 2017.
20. Sivasamy, R., et al., "Polarization-independent single-layer ultra-wideband frequency-selective surface," *International Journal of Microwave and Wireless Technologies*, Vol. 9, No. 1, 93–97, 2017.
21. Huang, H.-F., S.-F. Zhang, and Y.-H. Hu, "A novel frequency selective surface for ultra wideband antenna performance improvement," *2013 Proceedings of the International Symposium on Antennas & Propagation (ISAP)*, Vol. 2, IEEE, 2013.

22. Mighani, M. and A. Mallahzadeh, "New UWB Shielding with frequency selective surfaces," *Journal of Communication Engineering*, Vol. 6, No. 1, 71–80, 2017.
23. Ranga, Y., K. P. Esselle, and L. Matekovits, "Making UWB antennas unidirectional: Phase coherence with an ultra-wide band frequency selective surface reflector," *The World of Applied Electromagnetics*, 227–258, Springer, Cham, 2018.
24. Zhou, H., "Low-pass frequency selective surface with wideband high-stop response for shipboard radar," *Journal of Electromagnetic Waves and Applications*, Vol. 27, No. 1, 117–122, 2013.
25. Kesavan, A., R. Karimian, and T. A. Denidni, "A novel wideband frequency selective surface for millimeter-wave applications," *IEEE Antennas and Wireless Propagation Letters*, Vol. 15, 1711–1714, 2016.
26. Tripathy, M. R. and D. Ronnow, "A wideband frequency selective surface reflector for 4G/X-band/Ku-band," *Progress In Electromagnetics Research*, Vol. 81, 151–159, 2018.
27. Zhao, J. and Y. Cheng, "Ultrabroadband microwave metamaterial absorber based on electric SRR loaded with lumped resistors," *Journal of Electronic Materials*, Vol. 45, No. 10, 5033–5039, 2016.
28. Cheng, Y., et al., "Ultra-thin low-frequency broadband microwave absorber based on magnetic medium and metamaterial," *Journal of Electronic Materials*, Vol. 46, No. 2, 1293–1299, 2017.
29. Feng, J., et al., "An ultrathin polarization-independent wideband metamaterial absorber for EMC applications," *2017 International Symposium on Electromagnetic Compatibility-EMC EUROPE*, IEEE, 2017.
30. Li, W., et al., "Broadband composite radar absorbing structures with resistive frequency selective surface: Optimal design, manufacturing and characterization," *Composites Science and Technology*, Vol. 145, 10–14, 2017.
31. Laroussi, M. and J. Reece Roth, "Numerical calculation of the reflection, absorption, and transmission of microwaves by a nonuniform plasma slab," *IEEE Transactions on Plasma Science*, Vol. 21, No. 4, 366–372, 1993.
32. Vidmar, R. J., "On the use of atmospheric pressure plasmas as electromagnetic reflectors and absorbers," *IEEE Transactions on Plasma Science*, Vol. 18, No. 4, 733–741, 1990.
33. Stalder, K. R., R. J. Vidmar, and D. J. Eckstrom, "Observations of strong microwave absorption in collisional plasmas with gradual density gradients," *Journal of Applied Physics*, Vol. 72, No. 11, 5089–5094, 1992.
34. Anderson, T., et al., "Plasma frequency selective surfaces," *IEEE Transactions on Plasma Science*, Vol. 35, No. 2, 407–415, 2007.
35. Ghayekhloo, A., A. Abdolali, and S. H. M. Armaki, "Observation of radar cross-section reduction using low-pressure plasma-arrayed coating structure," *IEEE Transactions on Antennas and Propagation*, Vol. 65, No. 6, 3058–3064, 2017.
36. Yuan, C. X., Z. X. Zhou, J. W. Zhang, X. L. Xiang, Y. Feng, and H. G. Sun, "Properties of propagation of electromagnetic wave in a multilayer radar-absorbing structure with plasma-and radar-absorbing material," *IEEE Trans. Plasma Sci.*, Vol. 39, No. 9, 1768–1775, 2011.
37. Joozdani, M. Z. and M. K. Amirhosseini, "Wideband absorber with combination of plasma and resistive frequency selective surface," *IEEE Transactions on Plasma Science*, Vol. 44, No. 12, 3254–3261, 2016.
38. Ghayekhloo, A., M. Afsahi, and A. A. Orouji, "Checkerboard plasma electromagnetic surface for wideband and wide-angle bistatic radar cross section reduction," *IEEE Transactions on Plasma Science*, Vol. 45, No. 4, 603–609, 2017.
39. Rahmanzadeh, M., H. Rajabalipanah, and A. Abdolali, "Analytical investigation of ultrabroadband plasma-graphene radar absorbing structures," *IEEE Transactions on Plasma Science*, Vol. 45, No. 6, 945–954, 2017.
40. Lieberman, M. A. and A. J. Lichtenberg, *Principles of Plasma Discharges and Materials Processing*, John Wiley & Sons, 2005.
41. Singh, H., S. Antony, and R. M. Jha, "Plasma-based radar cross section reduction," *Plasma-based Radar Cross Section Reduction*, 1–46, Springer Singapore, 2016.

42. Costa, F., A. Monorchio, and G. Manara, "An overview of equivalent circuit modeling techniques of frequency selective surfaces and metasurfaces," *Appl. Comput. Electromagn. Soc. J.*, Vol. 29, No. 12, 960–976, 2014.
43. Joozdani, M. Z., M. K. Amirhosseini, and A. Abdolali, "Equivalent circuit model for frequency-selective surfaces embedded within a thick plasma layer," *IEEE Transactions on Plasma Science*, Vol. 43, No. 10, 3590–3598, 2015.
44. Yuan, C.-X., et al., "Properties of propagation of electromagnetic wave in a multilayer radar-absorbing structure with plasma-and radar-absorbing material," *IEEE Transactions on Plasma Science*, Vol. 39, No. 9, 1768–1775, 2011.
45. Stalder, K. R. and D. J. Eckstrom, "Afterglow decay kinetics of nonuniform plasmas with cylindrical symmetry: Application to the measurement of electron decay in large, photoionized plasmas in atmospheric-pressure helium," *Journal of Applied Physics*, Vol. 72, No. 9, 3917–3923, 1992.
46. Akhtar, K., et al., "Characterization of laser produced tetrakis (dimethylamino) ethylene plasma in a high-pressure background gas," *IEEE Transactions on Plasma Science*, Vol. 32, No. 2, 813–822, 2004.